NETWORKS AND HETEROGENEOUS MEDIA
©American Institute of Mathematical Sciences
Volume **12**, Number **4**, December **2017**

doi:10.3934/nhm.2017027

pp. **663–681**

CAPACITY DROP AND TRAFFIC CONTROL FOR A SECOND ORDER TRAFFIC MODEL

Oliver Kolb and Simone Göttlich

Department of Mathematics
University of Mannheim
68131 Mannheim, Germany

Paola Goatin

Inria Sophia Antipolis - Méditerranée
Université Côte d'Azur, Inria, CNRS, LJAD
06902 Sophia Antipolis Cedex, France

(Communicated by Benedetto Piccoli)

Abstract. In this paper, we illustrate how second order traffic flow models, in our case the Aw-Rascle equations, can be used to reproduce empirical observations such as the capacity drop at merges and solve related optimal control problems. To this aim, we propose a model for on-ramp junctions and derive suitable coupling conditions. These are associated to the first order Godunov scheme to numerically study the well-known capacity drop effect, where the outflow of the system is significantly below the expected maximum. Control issues such as speed and ramp meter control are also addressed in a first-discretize-then-optimize framework.

1. **Introduction.** The description of vehicular traffic flow based on systems of conservation or balance laws has been proposed by many researchers during the last decades, see for example [9, 30] and the references therein. In contrast to first order traffic models consisting only of one scalar equation for the traffic density, second order models are characterized by a second equation for the evolution of traffic mean velocity. Among these, Aw and Rascle [2] proposed a model that overcomes the drawbacks of previous models, and is capable to capture some traffic characteristics linked to the anticipation behavior of drivers. Greenberg [12] presented an extension of the Aw-Rascle model including a relaxation term towards a preferred (or equilibrium) velocity. Since then many contributions have appeared on theoretical and numerical investigations [1, 3, 4, 10], networked problems [8, 13, 15, 16, 26], and more recently phenomenological and data driven approaches [7, 17, 21, 24, 29].

In this work, we present results concerning the coupling of interlinked road networks to on-ramps. It is known that in such situations capacity drops occur for high traffic densities, see e.g. [13, 17, 21, 23, 29]. Capacity drop means that the measured outflow of the system is smaller than the expected maximal flow if the system is well utilized. The difference might be up to 10% or even higher [17, 29].

2010 *Mathematics Subject Classification.* 90B20, 35L65.

Key words and phrases. Traffic flow, second order model, on-ramp coupling, numerical simulations, optimal control.

The second author is supported by DFG grant GO 1920/4-1.

This can be explained by a less efficient driving style when exiting a congested zone (upstream the on-ramp), which reduces the downstream flow compared to free-flow conditions [30].

The coupling of on-ramps to roads is similar to the modeling of a merge [18]. However, in contrast to the majority of already existing approaches, here we assume that the on-ramp is given by an ordinary differential equation, see [6, 11]. For second order models, the challenge here is to find appropriate conditions to ensure the conservation of mass and momentum flow. Once these coupling conditions are defined, they can be integrated in a finite-volume type numerical scheme to compute the evolution of traffic conditions on the network. We use a first-order Godunov scheme combined with a time splitting to resolve the relaxation term. In particular, we observe that the model is able to reproduce the capacity drop effect for increasing inflows, similar to the study made in [13] and in contrast to [23], where the phenomenon is only observed for a short time period.

Furthermore, our approach gives the opportunity to consider questions of optimal control in a first-discretize-then-optimize framework. Typical control issues arising in the on-ramp context are speed limit and ramp metering. These kind of traffic flow control problems have been mainly studied in the context of first-order models based on the Lighthill-Whitham-Richards (LWR) equations [22], see e.g. [5, 11, 14, 25]. To the best of our knowledge, speed limit and ramp meter control has been not considered for the Aw-Rascle model so far. We discuss the numerical results obtained from the adjoint calculus and compare them to the LWR equations.

The outline is as follows: In Section 2 we present the Aw-Rascle model with relaxation term and the coupling conditions at on-ramps. Our discretization scheme will be introduced in Section 3. Numerical results concerning the capacity drop and optimal control issues can be found in Section 4. Comparisons to the solution of the LWR model are also given for all experiments.

2. Modeling.

We introduce the modeling equations given by the Aw-Rascle (AR) model [2] including a relaxation term as originally introduced in [12]. The model consists of a 2×2 system of conservation laws for the density and a sort of *generalized momentum* derived from the (anticipate) acceleration equation.

In this work, our focus is on the coupling of the Aw-Rascle model to on-ramps whose dynamics are modeled by ordinary differential equations. We will derive appropriate coupling conditions that allow for the definition of boundary conditions at junctions. As we will see in the numerical experiments, our modeling approach covers the capacity drop effect and allows to solve optimal control problems such as speed limit and ramp metering, cf. Section 4.3.

2.1. Road dynamics.

We briefly recall the Aw-Rascle traffic flow model [2] and explain how it can be extended to the context of networks. Traffic states are described by the density $\rho_i(x,t)$ and the mean speed of vehicles $v_i(x,t)$ on each road i at position x and time t.

Given some initial state $\big(\rho_i(x,0), v_i(x,0)\big)$ on each road i, the dynamics for $x \in (0, L_i)$ and $t \in (0,T)$ are described by [2, 12]

$$\partial_t \rho_i + \partial_x(\rho_i v_i) = 0, \tag{1}$$

$$\partial_t(\rho_i w_i) + \partial_x(\rho_i v_i w_i) = -\rho_i \frac{v_i - V_i(\rho_i)}{\delta}, \tag{2}$$

$$w_i = v_i + p_i(\rho_i), \tag{3}$$

or in conservative form with $y_i = \rho_i w_i$

$$\partial_t \begin{pmatrix} \rho_i \\ y_i \end{pmatrix} + \partial_x \begin{pmatrix} y_i - \rho_i p_i(\rho_i) \\ \big(y_i - \rho_i p_i(\rho_i)\big)\frac{y_i}{\rho_i} \end{pmatrix} = \underbrace{\begin{pmatrix} 0 \\ -\frac{(y_i - \rho_i p_i(\rho_i)) - \rho_i V_i(\rho_i)}{\delta} \end{pmatrix}}_{=g_i(\rho_i, y_i)}, \tag{4}$$

where $p_i(\rho)$ is a known pressure function satisfying $p_i'(\rho) > 0$ and $\rho p_i''(\rho) + 2p_i'(\rho) > 0$ for all ρ. The latter condition ensures that the curve $\{w_i(\rho, v) = v + p_i(\rho) \overset{!}{=} c\}$ for any constant $c > 0$ is strictly concave and passes through the origin of the $(\rho, \rho v)$-plane. Further, there exists a sonic point $\sigma_i(c)$ maximizing the flux ρv along the curve $\{w_i(\rho, v) = c\}$. The relaxation term in the velocity equation includes the preferential speed function $V_i(\rho)$ which the drivers tend to adopt and a relaxation parameter δ.

We consider the preferential velocity depending on the density,

$$V_i(\rho) = v_i^{\max}\left(1 - \frac{\rho}{\rho_i^{\max}}\right), \tag{5}$$

and the pressure function (as in [13, 23])

$$p_i(\rho) = \frac{v_i^{\mathrm{ref}}}{\gamma_i}\left(\frac{\rho}{\rho_i^{\max}}\right)^{\gamma_i} \tag{6}$$

equipped with maximal density $\rho_i^{\max} > 0$, maximal velocity $v_i^{\max} > 0$, reference velocity $v_i^{\mathrm{ref}} > 0$ and $\gamma_i > 0$. Later, in Section 4.3, we will also consider time dependent velocities $v_i^{\max}(t)$ and $v_i^{\mathrm{ref}}(t)$ so that actually $p_i(\rho) = p_i(\rho, t)$, $V_i(\rho) = V_i(\rho, t)$ and $g_i(\rho, y) = g_i(\rho, y, t)$.

Note that above and in the following, we use $w_i = w_i(x, t)$ as space and time dependent state variable but also as function, e.g. in the form $w_i(\rho, v, t) = v + p_i(\rho, t)$. Analogously, we will use the notation $v_i(U, t) = w - p_i(\rho, t)$ for the velocity of a state $U = (\rho, \rho w)$. Similar to first order traffic models, we define the demand and supply functions for each road i as follows: For a given constant c (corresponding to a fixed value of w) we have

$$D_i(\rho, c, t) = \begin{cases} \big(c - p_i(\rho, t)\big)\rho & \text{if } \rho \le \sigma_i(c, t), \\ \big(c - p_i(\sigma_i(c, t), t)\big)\,\sigma_i(c, t) & \text{if } \rho \ge \sigma_i(c, t), \end{cases} \tag{7}$$

$$S_i(\rho, c, t) = \begin{cases} \big(c - p_i(\sigma_i(c, t), t)\big)\,\sigma_i(c, t) & \text{if } \rho \le \sigma_i(c, t), \\ \big(c - p_i(\rho, t)\big)\rho & \text{if } \rho \ge \sigma_i(c, t), \end{cases} \tag{8}$$

where

$$\sigma_i(c, t) = \rho_i^{\max}\left(\frac{c\,\gamma_i}{v_i^{\mathrm{ref}}(t)\,(1 + \gamma_i)}\right)^{\frac{1}{\gamma_i}} \tag{9}$$

is the sonic point on the curve $\{w_i(\rho, v, t) = v + p_i(\rho, t) \overset{!}{=} c\}$ in the $(\rho, \rho v)$-plane. An illustration of the considered demand and supply functions is given in Figure 1. Supply and demand functions are needed to formulate the coupling of different roads or on-ramps. Note that due to the dependence on a given value of w, the value of the supply function at $\rho^{\max}$ may differ from zero. Even though this can be considered as a potential drawback of the applied model, the effect is compensated by the relaxation term to a great extent, since the latter forces the velocity and therewith the flux to zero when the density approaches $\rho^{\max}$.

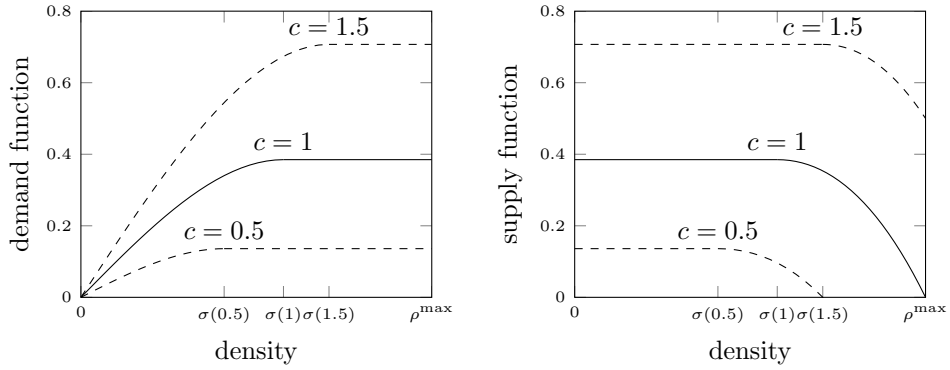

FIGURE 1. Demand and supply functions on a fixed road for $\rho^{\max} = 1$, $v^{\text{ref}} = 2$, $\gamma = 2$ and the given values for c.

2.2. **Coupling and boundary conditions.** In the following, we present the serial coupling between single roads as well as the coupling with an on-ramp. In general, for well-posed coupling conditions in networks of hyperbolic conservation laws, one considers (half-)Riemann problems defining the set of admissible states for each road at the junction, i.e., states such that all waves produced by the Riemann problem have negative/positive speed if the considered road is an incoming/outgoing road (cf. [13]). Under these constraints, the flow at the junction is maximized, where additional conditions have to be posed to achieve uniqueness of the solution. Those conditions as well as the flow maximization are already included in the following description.

The considered coupling and boundary conditions can be given in terms of mass flow $q = \rho v$ and "momentum flow" qw. The computation of the actual states at a junction is not necessary (cf. the discretization in Section 3). Different to other coupling conditions [13, 15, 18, 23, 26], we assume that in the situation of a merge the priority parameter P is independent of the demand of the ingoing roads. This guarantees the consistency of the corresponding Riemann solver, see [9, Definition 4.2.2].

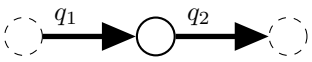

FIGURE 2. 1-to-1 junction.

1-to-1 junction. We use index 1 for the ingoing road, index 2 for the outgoing road, and consider the data $U_i = (\rho_i, \rho_i w_i)$ at the adjacent boundaries of roads 1 and 2, respectively. Note that we omit the time dependency of the states U_i and the fluxes q_i in the following for a better reading, whereas we still indicate the explicit time dependency of the demand and supply functions.

Flow maximization at the junction over all admissible states leads to

$$q_1 = q_2 = \tilde{q} = \min\left\{D_1\left(\rho_1, w_1, t\right),\ S_2\left(\tilde{\rho}_2, w_1, t\right)\right\}, \tag{10}$$

where $\tilde{\rho}_2$ is either obtained by the intersection of the curves

$$\{v_2(U,t) = v_2(U_2,t)\} \quad \text{and} \quad \{w_2(U,t) = w_1\}, \tag{11}$$

or $\tilde{\rho}_2 = 0$. Note that for the considered pressure functions this problem can be solved explicitly:

$$\tilde{\rho}_2 = \rho_2^{\max} \left(\max \left(\frac{\gamma_2}{v_2^{\mathrm{ref}}(t)} \big(w_1 - v_2(U_2, t)\big), 0 \right) \right)^{\frac{1}{\gamma_2}}. \tag{12}$$

Then, $q_1 = q_2 = \tilde{q}$ determines the mass flow out of road 1/into road 2. Further, with $\tilde{w} = w_1$ at the junction, the momentum flow is given by $\tilde{q}\tilde{w}$.

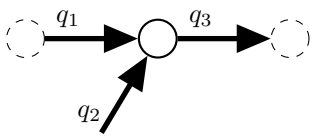

FIGURE 3. 1-to-1 junction with on-ramp.

On-ramp at a 1-to-1 junction. We consider a 1-to-1 junction with an on-ramp. Here, we use index 1 for the ingoing road, index 2 for the on-ramp, index 3 for the outgoing road, and consider the data $U_i = (\rho_i, \rho_i w_i)$ on roads 1 and 3, respectively, and the queue length l_2 at the on-ramp.

For the demand $D_2(l,t)$ at the on-ramp we apply

$$D_2(l,t) = u_2(t) \begin{cases} f_2^{\max} & \text{if } l > 0, \\ \min\{f_2^{\mathrm{in}}(t), f_2^{\max}\} & \text{if } l = 0, \end{cases} \tag{13}$$

where l is the length of the queue, $u_2(t) \in [0,1]$ is the (time-dependent) metering rate, $f_2^{\mathrm{in}}(t)$ the "inflow" of cars arriving at the on-ramp and $f_2^{\max}$ the maximum flow onto the main road.

To get a unique solution, we assign the priority parameter P to road 1, and apply

$$q_1 = \min\big\{D_1\big(\rho_1, w_1, t\big),\, \max\big\{PS_3\big(\tilde{\rho}_3, w_1, t\big),\, S_3\big(\tilde{\rho}_3, w_1, t\big) - D_2\big(l_2, t\big)\big\}\big\}, \tag{14}$$

$$q_2 = \min\big\{D_2\big(l_2, t\big),\, \max\big\{(1-P)S_3\big(\tilde{\rho}_3, w_1, t\big),\, S_3\big(\tilde{\rho}_3, w_1, t\big) - D_1\big(\rho_1, w_1, t\big)\big\}\big\}, \tag{15}$$

$$q_3 = q_1 + q_2, \tag{16}$$

where $\tilde{\rho}_3$ is either obtained by the intersection of the curves

$$\{v_3(U,t) = v_3(U_3,t)\} \quad \text{and} \quad \{w_3(U,t) = w_1\}, \tag{17}$$

or $\tilde{\rho}_3 = 0$. Again, the density $\tilde{\rho}_3$ can be computed explicitly:

$$\tilde{\rho}_3 = \rho_3^{\max} \left(\max \left(\frac{\gamma_3}{v_3^{\mathrm{ref}}(t)} \big(w_1 - v_3(U_3, t)\big), 0 \right) \right)^{\frac{1}{\gamma_3}}. \tag{18}$$

As before, the momentum flow is computed by multiplication of q_1 and q_3 with $\tilde{w} = w_1$, while the formal momentum flow $\tilde{w}q_2$ from the on-ramp does not influence the state of the on-ramp and is therefore not computed.

The evolution of the queue at the on-ramp is given by

$$\frac{d\, l_2(t)}{dt} = f_2^{\mathrm{in}}(t) - q_2, \tag{19}$$

where we typically start with empty queues, i.e., $l_2(0) = 0$.

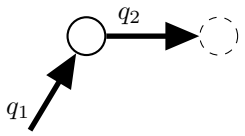

FIGURE 4. On-ramp at origin.

On-ramp at origin. We consider an on-ramp at a vertex with only one outgoing road. We use index 1 for the on-ramp with queue length l_1, and index 2 for the road with data $U_2 = (\rho_2, \rho_2 w_2)$.

Similar to above we apply

$$D_1(l,t) = u_1(t) \begin{cases} f_1^{\max} & \text{if } l > 0, \\ \min\{f_1^{\text{in}}(t), f_1^{\max}\} & \text{if } l = 0 \end{cases} \tag{20}$$

for the demand at the on-ramp, where l is the length of the queue, $u_1(t) \in [0,1]$ is the (time-dependent) metering rate, $f_1^{\text{in}}(t)$ the inflow of cars arriving at the on-ramp and $f_1^{\max}$ the maximum flow onto the road.

In this case there is no value for w to evaluate the supply function of the road, which is needed to determine the actual flux onto the road $\tilde{q}$ in a similar fashion as in the case of a simple 1-to-1 junction, i.e., similar to (10). Therefore, we consider an auxiliary left state U_1 mimicking the desired inflow of the on-ramp. We assume that the velocity of the auxiliary state is at equilibrium with respect to the desired velocity of the road, i.e., we search for a state

$$U_1 = \big(\rho, \rho\tilde{w}\big) \qquad \text{such that} \qquad \rho V_2(\rho, t) = D_1(l,t), \tag{21}$$

where $\tilde{w} = w_2(\rho, V_2(\rho,t), t)$. Assuming that the flux $D_1(l,t) \le f_1^{\max}$ can be realized with the velocity function V_2, we get the solutions

$$\rho_\pm = \frac{\rho_2^{\max}}{2} \pm \sqrt{\frac{(\rho_2^{\max})^2}{4} - \frac{\rho_2^{\max} D_1(l,t)}{v_2^{\max}(t)}}. \tag{22}$$

Here we choose ρ_-, since this choice also fulfils

$$D_2(\rho_-, \tilde{w}, t) = D_1(l,t). \tag{23}$$

Finally, we apply

$$q_1 = q_2 = \tilde{q} = \min\big\{D_1(l_1,t),\, S_2\big(\tilde{\rho}_2, \tilde{w}, t\big)\big\} \tag{24}$$

with $\tilde{w} = w_2(\rho_-, V_2(\rho_-,t),t)$, and $\tilde{\rho}_2$ is either obtained by the intersection of the curves

$$\{v_2(U,t) = v_2(U_2,t)\} \quad \text{and} \quad \{w_2(U,t) = \tilde{w}\}, \tag{25}$$

or $\tilde{\rho}_2 = 0$. The explicit representation is the same as (12).

Similar to above, the evolution of the queue at the on-ramp is given by

$$\frac{d\,l_1(t)}{dt} = f_1^{\text{in}}(t) - q_1. \tag{26}$$

FIGURE 5. Outflow at a vertex.

Outflow conditions. At nodes with only one ingoing road (with index 1) we consider absorbing boundary conditions up to a given maximum flow rate $f_1^{\text{out}}(t)$:

$$q_1 = \min\left\{D_1(\rho_1, w_1, t),\, f_1^{\text{out}}(t)\right\}. \tag{27}$$

The momentum flow is given by $q_1 w_1$.

3. **Discretization.** For the numerical solution of the described model, a finite number of time points $t^n = n\Delta t$ is considered, where $\Delta t = T/Nt$. Further, each road i is divided into Nx_i cells of equal size $\Delta x_i = L_i/Nx_i$. To fulfill the CFL condition, we will claim (at least) $\Delta t\, v_i^{\max} \le \Delta x_i$ in all numerical examples.

3.1. **Roads.** The underlying balance law (4) is discretized with a fractional step method: We use a first order Godunov scheme for the flux term and an implicit Euler method for the relaxation term. Due to the fundamental idea of the Godunov scheme, the computation of the actual states at junctions is not necessary and the coupling will be given in terms of fluxes only. Note that in the following $U_i = (\rho_i, \rho_i w_i)$ denotes again the state.

On each road i the initial conditions (for $j \in \{1, \dots, Nx_i\}$) are given by the cell averages

$$U^0_{i,j-0.5} = \frac{1}{\Delta x_i} \int_{(j-1)\Delta x_i}^{j\Delta x_i} U_i(x, 0)\, dx. \tag{28}$$

Then, for $n \in \{0, \dots, Nt-1\}$ and $j \in \{1, \dots, Nx_i\}$ we apply

$$\tilde{U}^{n+1}_{i,j-0.5} = U^n_{i,j-0.5} - \frac{\Delta t}{\Delta x_i}\left(F^n_{i,j} - F^n_{i,j-1}\right), \qquad \text{(transport)} \tag{29}$$

$$U^{n+1}_{i,j-0.5} = \tilde{U}^{n+1}_{i,j-0.5} + \Delta t\, g(U^{n+1}_{i,j-0.5}). \qquad \text{(relaxation term)} \tag{30}$$

The flux terms $F^n_{i,0}$ and F^n_{i,Nx_i} are given via coupling/boundary conditions (see next subsection) and for $j \in \{1, \dots, Nx_i - 1\}$ we have

$$F^n_{i,j} = \begin{pmatrix} q^n_{i,j} \\ w^n_{i,j-0.5}\, q^n_{i,j} \end{pmatrix} \tag{31}$$

with

$$q^n_{i,j} = \min\left(D_i(\rho^n_{i,j-0.5}, w^n_{i,j-0.5}, t^n),\, S_i(\tilde{\rho}^n_{i,j}, w^n_{i,j-0.5}, t^n)\right), \tag{32}$$

where $\tilde{\rho}^n_{i,j}$ is either obtained by the intersection of the curves

$$\{v_i(U, t^n) = v^n_{i,j+0.5}\} \quad \text{and} \quad \{w_i(U, t^n) = w^n_{i,j-0.5}\}, \tag{33}$$

or $\tilde{\rho}^n_{i,j} = 0$. Note that this treatment is consistent with the treatment of a 1-to-1 junction where two roads with the same parameters meet.

3.2. **Coupling and boundary conditions.** We complete the numerical scheme by the description of the coupling and boundary conditions according to the model equations from Section 2.2. As already mentioned, we only need the coupling fluxes here and not the actual states at the junctions.

1-to-1 junction. As before, we use index 1 for the ingoing road and index 2 for the outgoing road. According to (10) we apply for $n \in \{0, \dots, Nt-1\}$

$$\tilde{q}^n = \min\left\{ D_1\left(\rho^n_{1,Nx_1-0.5}, w^n_{1,Nx_1-0.5}, t^n\right),\ S_2\left(\tilde{\rho}^n_{2,0}, w^n_{1,Nx_1-0.5}, t^n\right)\right\}, \tag{34}$$

where $\tilde{\rho}^n_{2,0}$ is either obtained by the intersection of the curves

$$\{v_2(U,t^n) = v^n_{2,0.5}\} \quad \text{and} \quad \{w_2(U,t^n) = w^n_{1,Nx_1-0.5}\}, \tag{35}$$

or $\tilde{\rho}^n_{2,0} = 0$. Due to the choice of the pressure function (6), $\tilde{\rho}^n_{2,0}$ can be directly computed according to (12). Finally, we get

$$F^n_{1,Nx_1} = F^n_{2,0} = \begin{pmatrix} \tilde{q}^n \\ w^n_{1,Nx_1-0.5}\,\tilde{q}^n \end{pmatrix}. \tag{36}$$

On-ramp at a 1-to-1 junction. We use index 1 for the ingoing road, index 2 for the on-ramp and index 3 for the outgoing road. According to (13) we apply

$$\tilde{D}_2(l,t) = u_2(t)\min\left\{ f^{\text{in}}_2(t) + \frac{l}{\Delta t}, f^{\max}_2 \right\} \tag{37}$$

for the demand at the on-ramp. Then, using the abbreviations

$$d^n_1 = D_1\left(\rho^n_{1,Nx_1-0.5}, w^n_{1,Nx_1-0.5}, t^n\right), \tag{38}$$

$$d^n_2 = \tilde{D}_2(l^n_2, t^n), \tag{39}$$

$$s^n_3 = S_3\left(\tilde{\rho}^n_{3,0}, w^n_{1,Nx_1-0.5}, t^n\right), \tag{40}$$

we get from (14) and (15)

$$q^n_1 = \min\left\{d_1,\ \max\left\{Ps_3,\ s_3 - d_2\right\}\right\}, \tag{41}$$

$$q^n_2 = \min\left\{d_2,\ \max\left\{(1-P)s_3,\ s_3 - d_1\right\}\right\}, \tag{42}$$

$$q^n_3 = q^n_1 + q^n_2, \tag{43}$$

where $\tilde{\rho}^n_{3,0}$ is either obtained by the intersection of the curves

$$\{v_3(U,t^n) = v^n_{3,0.5}\} \quad \text{and} \quad \{w_3(U,t^n) = w^n_{1,Nx_1-0.5}\}, \tag{44}$$

or $\tilde{\rho}^n_{3,0} = 0$. Again, in our case a direct computation is possible due to (18). Finally, we have

$$F^n_{1,Nx_1} = \begin{pmatrix} q^n_1 \\ w^n_{1,Nx_1-0.5}\,q^n_1 \end{pmatrix}, \quad F^n_{3,0} = \begin{pmatrix} q^n_3 \\ w^n_{1,Nx_1-0.5}\,q^n_3 \end{pmatrix} \tag{45}$$

and apply

$$l^{n+1}_2 = l^n_2 + \Delta t\left(f^{\text{in}}_2(t^n) - q^n_2\right) \tag{46}$$

for the update of the queue length via the explicit Euler scheme. Note that we always achieve a non-negative queue length by our choice of the demand function (37). Alternatively, the time step Δt could be adapted, cf. [6].

On-ramp at origin. We use index 1 for the on-ramp and index 2 for the road. Similar to above we apply

$$\tilde{D}_1(l,t) = u_1(t)\min\left\{ f^{\text{in}}_1(t) + \frac{l}{\Delta t}, f^{\max}_1 \right\} \tag{47}$$

for the demand at the on-ramp. Next, following the idea introduced in Section 2.2, we compute

$$\rho^n_{1,-} = \frac{\rho^{\max}_2}{2} - \sqrt{\frac{(\rho^{\max}_2)^2}{4} - \frac{\rho^{\max}_2 \tilde{D}_1(l^n_1, t^n)}{v^{\max}_2(t^n)}} \tag{48}$$

and

$$\tilde{q}^n = \min\left\{\tilde{D}_1(l_1^n, t^n),\ S_2\big(\tilde{\rho}_{2,0}^n, \tilde{w}^n, t^n\big)\right\} \tag{49}$$

with $\tilde{w}^n = w_2(\rho_{1,-}^n, V_2(\rho_{1,-}^n, t^n), t^n)$, and $\tilde{\rho}_{2,0}^n$ is either obtained by the intersection of the curves

$$\{v_2(U,t) = v_{2,0.5}^n\} \quad \text{and} \quad \{w_2(U,t^n) = \tilde{w}^n\}, \tag{50}$$

or $\tilde{\rho}_{2,0}^n = 0$. Again, $\tilde{\rho}_{2,0}^n$ can be computed explicitly according to (12). Finally, we use

$$F_{2,0}^n = \begin{pmatrix} \tilde{q}^n \\ \tilde{w}^n\ \tilde{q}^n \end{pmatrix} \tag{51}$$

and apply

$$l_1^{n+1} = l_1^n + \Delta t\left(f_1^{\text{in}}(t^n) - \tilde{q}^n\right) \tag{52}$$

for the update of the queue length. Again, non-negativity of the queue length is ensured by our choice of the demand function (47).

Outflow conditions. At nodes with only one ingoing road (with index 1) we apply according to (27)

$$F_{1,Nx_1}^n = \begin{pmatrix} q_1^n \\ w_{1,Nx_1-0.5}^n\ q_1^n \end{pmatrix} \tag{53}$$

with

$$q_1^n = \min\left\{D_1\big(\rho_{1,Nx_1-0.5}^n, w_{1,Nx_1-0.5}^n, t^n\big),\ f_1^{\text{out}}(t^n)\right\}. \tag{54}$$

In the next section, we present a numerical study to show the characteristics of our modeling approach. We also comment on already existing examples from the literature, pointing out differences and similarities.

4. Numerical results.

Our numerical results emphasize on three different scenarios that our approach is able to deal with from a modeling and computational point of view. First, we show that, for a single road, the Aw-Rascle (AR) model with relaxation term numerically converges to the Lighthill-Whitham-Richards (LWR) model as expected [12]. The second example considers the capacity drop for a 1-to-1 junction with on-ramp. We will see that this phenomenon is not covered by the classical LWR model. The third example tackles speed control and coordinated ramp metering control issues. It will turn out that the control strategies considered individually do not lead to the best possible travel times, while the combination of both lead to satisfying results.

4.1. Aw-Rascle towards LWR.

We consider a single road as depicted in Figure 6 with length $L = 1\,\text{km}$, $\rho^{\max} = 200\,\frac{\text{cars}}{\text{km}}$, $v^{\max} = v^{\text{ref}} = 100\,\frac{\text{km}}{\text{h}}$ and $\rho_0 = 80\,\frac{\text{cars}}{\text{km}}$ as initial density. For the AR model we further use $\gamma = 2$, $v_0 = 60\,\frac{\text{km}}{\text{h}}$ (in equilibrium state) and decreasing values for the relaxation parameter δ starting from a usual value of $\delta = 0.005$ hours (18 seconds, see e.g. [14]).

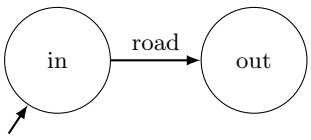

FIGURE 6. A single road.

We consider a simulation time of $T = 36$ seconds and

$$f^{\text{in}}(t) = \begin{cases} 4000 + 800\cos(4\pi\frac{t}{T}) & \text{for } 0 \le t \le \frac{T}{2}, \\ 4800 & \text{otherwise} \end{cases}$$

as inflow profile at the origin "in" (in $\frac{\text{cars}}{\text{h}}$). As discretization parameters, we apply $\Delta x = 10$ meters and $\Delta t = 0.18$ seconds.

Figure 7 shows density and velocity profiles on the whole road after 36 seconds. As expected, the solution of the Aw-Rascle model with relaxation term tends towards the LWR model for decreasing relaxation parameter δ. Moreover, decreasing densities are correlated with increasing velocities. Note that the application of larger values for the parameter γ in the pressure term leads to higher peaks in the simulation results (not shown here).

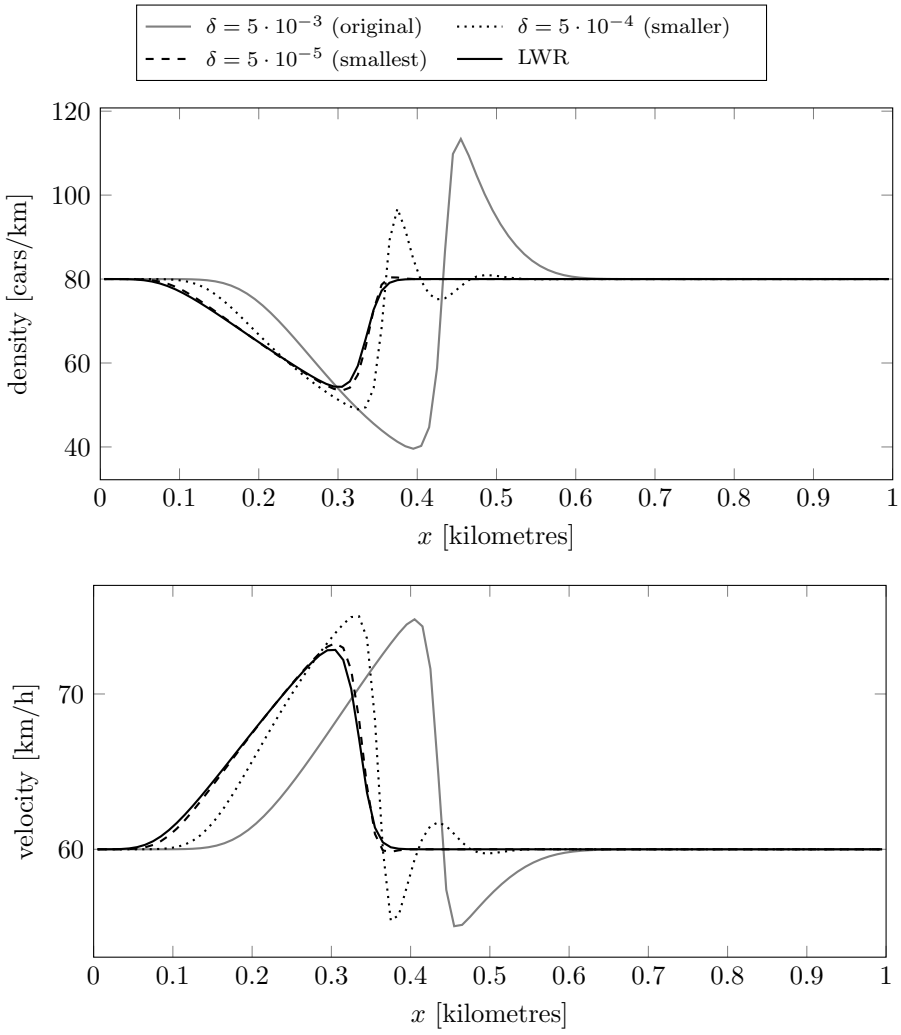

FIGURE 7. Density (top) and velocity (bottom) after 36 seconds for different choices of the relaxation parameter δ and for the LWR model.

4.2. **Capacity drop.** Now we turn our attention to study the capacity drop effect, cf. [13]. We will see that increasing the inflow into the network depicted in Figure 8 will at a certain point lead to a decreasing outflow. Thus, a significant difference between the effective and maximal possible outflow occurs in the Aw-Rascle model. Conversely, this effect is not captured by the classical LWR model. This is due to the different modeling of the supply function. In the congested regime, the value of the supply function is at its maximum in the LWR model and therefore no capacity drop occurs. However, in the AR model, the supply function additionally depends on the "incoming" value of w that allows for a different behavior.

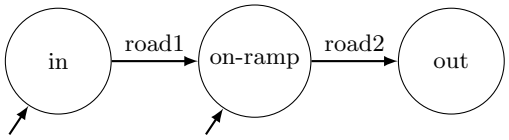

FIGURE 8. Two roads with an on-ramp in between.

We consider two roads of 1 km length with an on-ramp in between, see Figure 8. On both roads we use $\rho^{\max} = 180\,\frac{\text{cars}}{\text{km}}$, $v^{\max} = v^{\text{ref}} = 100\,\frac{\text{km}}{\text{h}}$, $\gamma = 2$, $\delta = 0.005\,\text{h}$ and an initial density of $50\,\frac{\text{cars}}{\text{km}}$. At the origin "in" we consider a constant (desired) inflow $f_1^{\text{in}} = 3500\,\frac{\text{cars}}{\text{h}}$. At the on-ramp we consider different (desired) inflows, starting from $f_2^{\text{in}} = 500\,\frac{\text{cars}}{\text{h}}$ up to $2500\,\frac{\text{cars}}{\text{h}}$ and down to $500\,\frac{\text{cars}}{\text{h}}$ again. As priority parameter at the on-ramp we use $P = 0.5$.

Table 1 and Figure 9 show the simulation results for the AR and the LWR model (with $\Delta x = 100$ metres and $\Delta t = 1.8$ seconds), i.e., the resulting stationary states. The first two columns report the desired and the actual inflow at the on-ramp. The following three values are the resulting density, velocity and the value of w just upstream the on-ramp (end of the first road). The last two columns show the total outflow at the end of the second road.

TABLE 1. Capacity drop effect

inflow at on-ramp in $[\frac{\text{cars}}{\text{h}}]$		ρ_1	v_1	w_1	outflow AR	outflow LWR
desired	actual	in $[\frac{\text{cars}}{\text{km}}]$	in $[\frac{\text{km}}{\text{h}}]$	in $[\frac{\text{km}}{\text{h}}]$	in $[\frac{\text{cars}}{\text{h}}]$	in $[\frac{\text{cars}}{\text{h}}]$
500	500	47.6	73.6	77.1	4000	4000
1000	1000	47.6	73.6	77.1	4500	4500
1500	1500	156.4	13.1	50.9	3554	4500
2000	1764	160.2	11.0	50.6	3527	4500
2500	1764	160.2	11.0	50.6	3527	4500
1000	1000	148.0	17.8	51.6	3629	4500
500	500	137.2	23.8	52.8	3762	4000

We begin with the interpretation of the results obtained from the AR model: Obviously, up to an inflow of $1000\,\frac{\text{cars}}{\text{h}}$ at the on-ramp, the total inflow (of $4500\,\frac{\text{cars}}{\text{h}}$) is within the capacity of the given road. When the inflow at the on-ramp further increases, the resulting total flux cannot be realized at some point. From then on, the value of w at the end of the first road directly influences the total flux entering the second road (compare equations (14) and (15) and the definition of the supply function (8)). As a consequence, the outflow at the end of the second road for the cases $f_2^{\text{in}} \in \{1500\,\frac{\text{cars}}{\text{h}}, 2000\,\frac{\text{cars}}{\text{h}}, 2500\,\frac{\text{cars}}{\text{h}}\}$ is lower than the outflow for the cases

$f_2^{\text{in}} \in \{500\,\frac{\text{cars}}{\text{h}}, 1000\,\frac{\text{cars}}{\text{h}}\}$. Due to the choice of the priority parameter $P = 0.5$, the effect of a decreasing outflow while the desired inflow increases stagnates as soon as the fluxes from the first road and the on-ramp are equal, which is the case for $f_2^{\text{in}} \in \{2000\,\frac{\text{cars}}{\text{h}}, 2500\,\frac{\text{cars}}{\text{h}}\}$.

Interestingly, even when the desired inflow at the on-ramp is lowered again, the original state for the same values of f_1^{in} and f_2^{in} is not reached. This is due to the fact that the outflow in the congested situation is below the accumulated desired inflows. Accordingly, the queue at the origin permanently increases in the final situation even though the capacity of the road could handle the desired inflows in the free flow situation.

Note that compared to the existing literature the capacity drop is investigated for different situations. In [13] no relaxation term is considered but a similar result is obtained. The construction principle for the capacity drop is the same (decreasing value of w for increasing flux), but in our investigations the possible equilibrium states are restricted due to the relaxation term so that higher densities on the incoming road lead to lower velocities (in difference to the equilibria 3 and 5 in [13, Table 3]). In [23], where a different junction model and also a different numerical scheme is used, the capacity drop effect for the model with relaxation term is only observed for short time intervals, whereas we identify a permanent drop, cf. Figure 9.

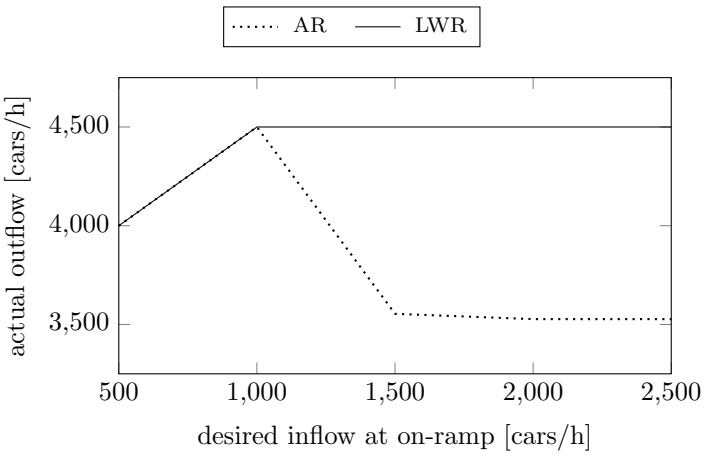

FIGURE 9. Actual outflow depending on the desired inflow at the on-ramp for the AR and the LWR model.

Finally, considering the same scenario with the LWR model (see [11] for the details), one observes that the outflow increases with the accumulated desired inflows until it reaches the maximum capacity of $4500\,\frac{\text{cars}}{\text{h}} = \frac{\rho^{\max}}{2} \cdot \frac{v^{\max}}{2}$ (see again Table 1 and Figure 9). According to the chosen priority $P = 0.5$, the actual inflows at the origin and at the on-ramp are $2250\,\frac{\text{cars}}{\text{h}}$ in that situation. Any further increase of the desired inflow at the on-ramp does not have any effect on the situation on the roads. Further, unlike the AR model, a decrease of the desired inflow f_2^{in} below $1000\,\frac{\text{cars}}{\text{h}}$ leads back to the original situation (as soon as the queues have emptied).

4.3. **Coordinated speed control and ramp metering.** For optimization purposes, we are finally interested in controlling maximal speed limits as well as on-ramp inflows to minimize the total travel time. As already introduced in equations (13) and (20), the ramp metering rate $u_i(t)$ is used to control the demand at the on-ramp. Similar to our recent work [11], we will use $v_i^{\max} = v_i^{\max}(t) \in [v_i^{\text{low}}, v_i^{\text{high}}]$ as another time-dependent (piecewise constant) control variable so that actually $V_i(\rho) = V_i(\rho, t)$ and $g_i(\rho, y) = g_i(\rho, y, t)$ for the relaxation term. Regarding the influence of the pressure term, we will consider two variants:

1. $v_i^{\text{ref}}(t) = v_i^{\max}(t)$, i.e., the pressure term directly depends on the (controllable) speed limit and therefore $p_i(\rho) = p_i(\rho, t)$;
2. $v_i^{\text{ref}}(t) = v_i^{\text{high}}$, i.e., the pressure term is independent of the current speed limit in the sense that $\frac{\partial p_i}{\partial v_i^{\max}} = 0$.

For our investigations, we consider the road network depicted in Figure 10 (adapted from [14]) with the road parameters of Table 2. The exponents in the pressure function are $\gamma_i = \gamma = 2$ for all roads and $\delta = 0.005\,\text{h}$ for the relaxation parameter. The priority parameter P at the on-ramp equals 0.5 and $f^{\max} = 2000\,\frac{\text{cars}}{\text{h}}$. At the origin "in" we consider $f^{\max} = 4000\,\frac{\text{cars}}{\text{h}}$.

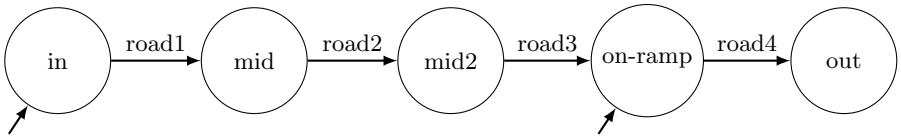

FIGURE 10. Road network with an on-ramp at the node "on-ramp".

TABLE 2. Properties of the roads in Figure 10

road	length [km]	$\rho^{\max}$ $[\frac{\text{cars}}{\text{km}}]$	v^{low} $[\frac{\text{km}}{\text{h}}]$	v^{high} $[\frac{\text{km}}{\text{h}}]$	initial density $[\frac{\text{cars}}{\text{km}}]$
road1	2	180	100	100	50
road2	1	180	50	100	50
road3	1	180	50	100	50
road4	2	180	100	100	50

We consider a time horizon of $T = 3.0$ hours and the boundary conditions shown in Figure 11. For the given scenario, we are interested in minimizing the total travel time

$$\sum_{\text{roads } i} \int_0^T \int_0^{L_i} \rho_i(x,t)\,dx\,dt \;+\; \sum_{\text{on-ramps } j} \int_0^T l_j(t)\,dt\,, \tag{55}$$

given an upper bound of 100 vehicles in the queue of the on-ramp. To solve this optimization task, we apply a first-discretize-then-optimize approach and adjoint calculus, see also [11]. Thus, for given control decisions (speed limits and metering rates), the discretization scheme described in Section 3 is always used to evaluate the objective function (55) (using the trapezoidal rule for quadrature). Further, sensitivity/gradient information with respect to the control decisions is computed based on the same discretization (we refer to [19, 20] for more details). Finally, the SQP solver DONLP2 [27, 28] is used for the optimization of the control decisions. The applied discretization parameters are $\Delta x = 250$ meters and $\Delta t = 7.2$ seconds.

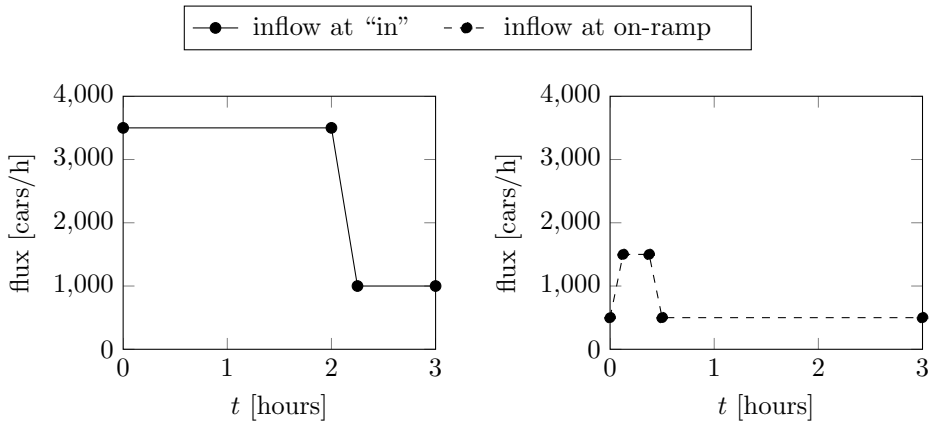

FIGURE 11. Inflow profiles for the network in Figure 10.

Table 3 shows the total travel times for the different models with and without optimization. The resulting queues for the AR model with scaling of the pressure function ($\frac{\partial p_i}{\partial v_i^{\max}} \neq 0$) are shown in Figure 12. Without ramp metering and speed control the queue at the on-ramp stays empty whereas more than 300 cars accumulate in the queue at the origin. When only ramp metering is considered, the queue at the origin is reduced to zero, while up to 100 cars accumulate in the queue at the on-ramp. Obviously, the prescribed upper bound for the queue at the on-ramp is active, impeding further improvement of the objective function. When ramp metering and speed control are used, the upper bound of 100 cars is even never touched. In the case of speed control only, the queue at the on-ramp stays empty, whereas the queue at the origin cannot be kept empty during the complete time horizon.

TABLE 3. Optimization results for the network in Figure 10

	AR, $\frac{\partial p_i}{\partial v_i^{\max}} \neq 0$	AR, $\frac{\partial p_i}{\partial v_i^{\max}} = 0$	LWR
no control	1871.7	1871.7	834.9
ramp metering only	1325.3	1325.3	834.9
speed control only	1122.8	872.6	834.9
both control types	814.5	818.4	834.9

Note that the results for the model without scaling of the pressure function ($\frac{\partial p_i}{\partial v_i^{\max}} = 0$) are quite similar considering the queues and therefore are not plotted. Nevertheless the possible improvement with respect to total travel time is much larger in the case of speed control only (872.6 versus 1122.8). Concerning the LWR model, both queues stay empty during the whole time horizon already in the uncontrolled case and the optimization procedure terminates directly in the other cases - leading to the same result. The optimality of the uncontrolled case with respect to total travel time results from the fact that the classical LWR model does not capture the capacity drop effect (cf. Section 4.2).

Figure 13 exemplarily shows where the improvement in total travel time comes from in the case of coordinated ramp metering and speed control in the model with scaling of the pressure function: The outflow of the system (plot on the right) in

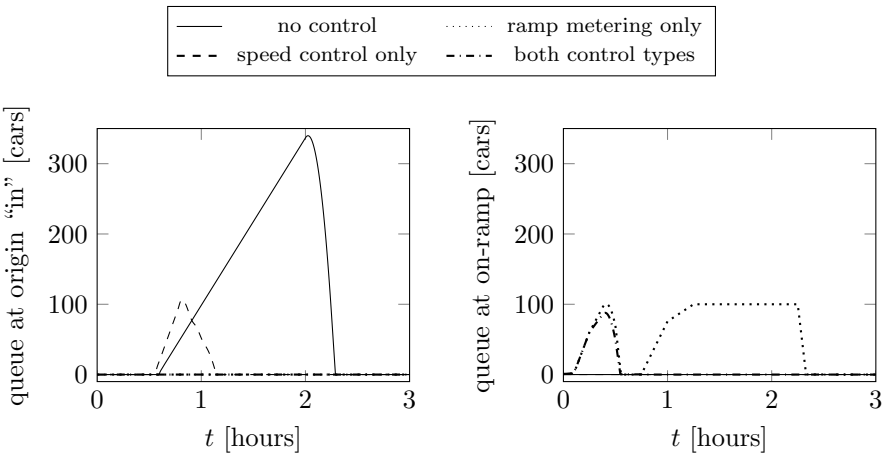

FIGURE 12. Queue at the origin "in" and the on-ramp with and without optimization.

the optimized scenario is permanently above the outflow of the uncontrolled system until it drops to the low inflow level after two hours. Figure 14 shows the applied (optimal) controls.

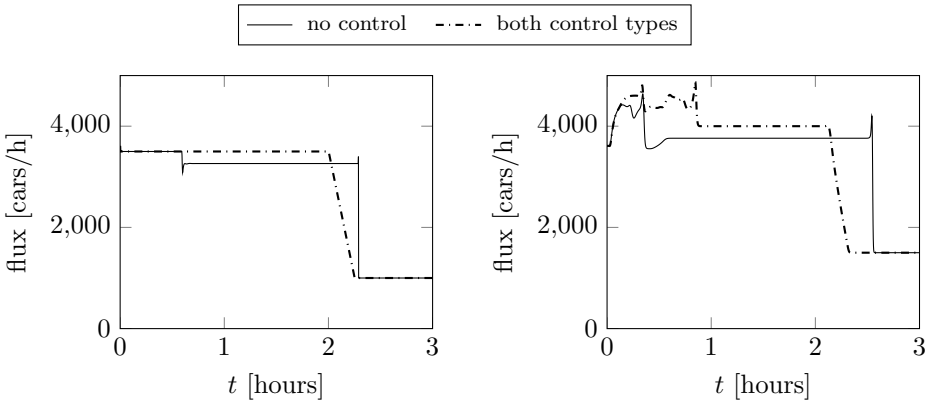

FIGURE 13. Flow at the origin "in" of the network (left) and at the node "out" (right) with and without optimization.

As shown in Table 3, the uncontrolled case is already optimal for the LWR model, i.e., no ramp metering or speed control is required. Accordingly, we take a look at the influence of the relaxation parameter δ within the second order model, which regulates the acceleration towards the desired velocity $V(\rho, t)$ of the LWR model.

Table 4 shows the simulation and optimization results for a wide choice of δ (on all roads). Since smaller values of δ lead to larger values for the acceleration towards the desired velocity, one would expect that the results for small values of δ get close to the results of the LWR model (as in Section 4.1). Surprisingly, it is the other way around for the considered scenario.

First, one observes larger total travel times in the case of smaller values for δ. These result from the faster reaction of the velocity on the increase in density behind

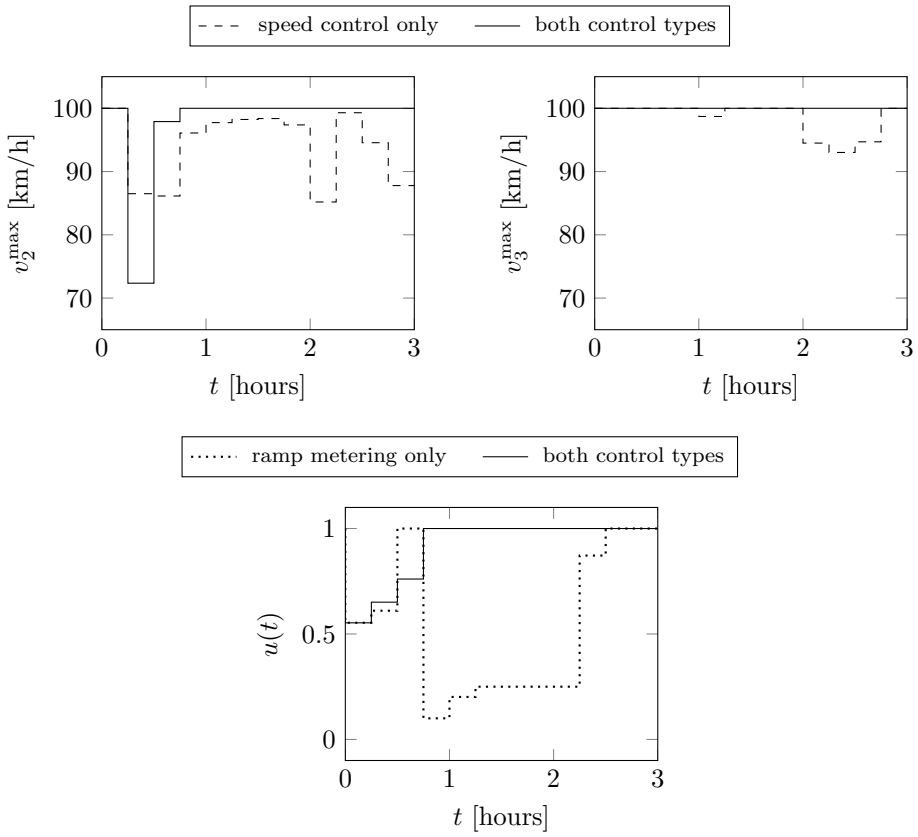

FIGURE 14. Optimal control of $v_i^{\max}(t)$ on road2 (top left) and road3 (top right) and $u(t)$ at the on-ramp (bottom).

TABLE 4. Total travel time for different choices of the relaxation parameter δ

δ	no control	opt. control, $\frac{\partial p_i}{\partial v_i^{\max}} \neq 0$	opt. control, $\frac{\partial p_i}{\partial v_i^{\max}} = 0$
$5 \cdot 10^{-5}$	2199.4	868.8	953.4
$5 \cdot 10^{-4}$	2137.1	860.1	856.3
$5 \cdot 10^{-3}$	1871.7	814.5	818.4
$5 \cdot 10^{-2}$	731.4	731.4	731.4
$5 \cdot 10^{-1}$	725.9	725.9	725.9

the on-ramp at the beginning of the scenario, which in turn accelerates the increase in density compared to the other parameter choices (see Figure 15 where the results for the case $\frac{\partial p_i}{\partial v_i^{\max}} \neq 0$ are plotted). For very large values of δ there is almost no reaction of the velocity on the density increase and no congestion. Qualitatively, the corresponding results are quite similar to the results of the LWR model (see again Figure 15).

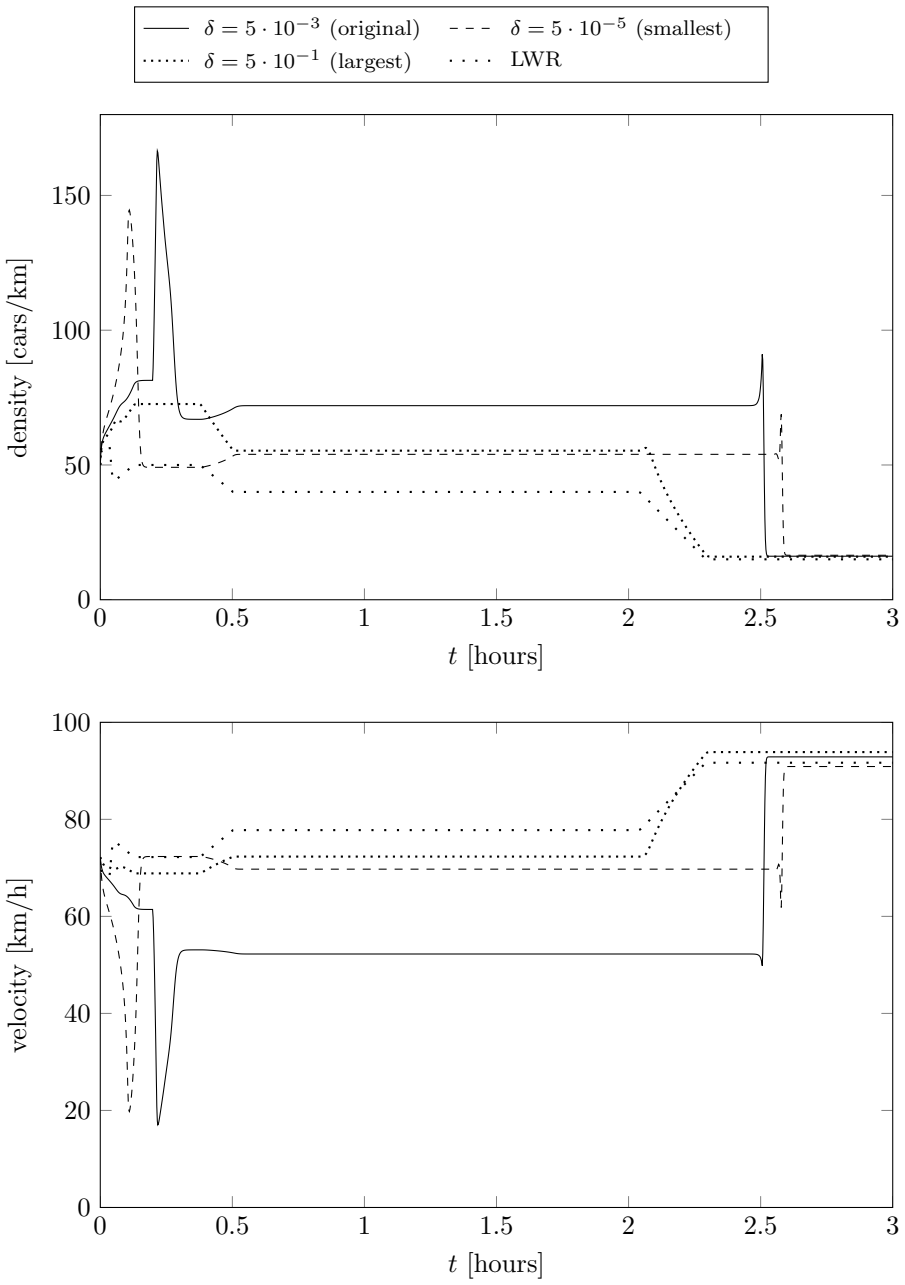

FIGURE 15. Density (top) and velocity (bottom) behind the on-ramp in the uncontrolled case for different choices of the relaxation parameter δ and for the LWR model.

5. **Conclusion.** In this work, we have set up coupling conditions for the Aw-Rascle model linked to on-ramps described by ordinary differential equations. Applying a first order Godunov scheme, the presented approach allows for numerical investigations of the capacity drop effect and optimal control problems.

Future work will include extensions to on-ramps that are described by first order traffic models such as the LWR model. We will derive appropriate coupling conditions and focus on theoretical properties.

REFERENCES

[1] A. Aw, A. Klar, T. Materne and M. Rascle, Derivation of continuum traffic flow models from microscopic follow-the-leader models, *SIAM Journal on Applied Mathematics*, **63** (2002), 259–278.

[2] A. Aw and M. Rascle, Resurrection of "second order" models of traffic flow, *SIAM Journal on Applied Mathematics*, **60** (2000), 916–938.

[3] F. Berthelin, P. Degond, M. Delitala and M. Rascle, A model for the formation and evolution of traffic jams, *Archive for Rational Mechanics and Analysis*, **187** (2008), 185–220.

[4] C. Chalons and P. Goatin, Transport-equilibrium schemes for computing contact discontinuities in traffic flow modeling, *Communications in Mathematical Sciences*, **5** (2007), 533–551.

[5] M. L. Delle Monache, B. Piccoli and F. Rossi, Traffic Regulation via Controlled Speed Limit, *SIAM Journal on Control and Optimization*, **55** (2017), 2936–2958.

[6] M. L. Delle Monache, J. Reilly, S. Samaranayake, W. Krichene, P. Goatin and A. M. Bayen, A PDE-ODE model for a junction with ramp buffer, *SIAM Journal on Applied Mathematics*, **74** (2014), 22–39.

[7] S. Fan, M. Herty and B. Seibold, Comparative model accuracy of a data-fitted generalized Aw-Rascle-Zhang model, *Networks and Heterogeneous Media*, **9** (2014), 239–268.

[8] M. Garavello and B. Piccoli, Traffic flow on a road network using the Aw-Rascle model, *Communications in Partial Differential Equations*, **31** (2006), 243–275.

[9] M. Garavello and B. Piccoli, *Traffic Flow on Networks*, Springfield, MO: American Institute of Mathematical Sciences (AIMS), 2006.

[10] P. Goatin, The Aw-Rascle vehicular traffic flow model with phase transitions, *Mathematical and Computer Modelling*, **44** (2006), 287–303.

[11] P. Goatin, S. Göttlich and O. Kolb, Speed limit and ramp meter control for traffic flow networks, *Engineering Optimization*, **48** (2016), 1121–1144.

[12] J. M. Greenberg, Extensions and amplifications of a traffic model of Aw and Rascle, *SIAM Journal on Applied Mathematics*, **62** (2001), 729–745.

[13] B. Haut and G. Bastin, A second order model of road junctions in fluid models of traffic networks, *Networks and Heterogeneous Media*, **2** (2007), 227–253.

[14] A. Hegyi, B. D. Schutter and H. Hellendoorn, Optimal coordination of variable speed limits to suppress shock waves, *IEEE Transactions on Intelligent Transportation Systems*, **6** (2005), 102–112.

[15] M. Herty, S. Moutari and M. Rascle, Optimization criteria for modelling intersections of vehicular traffic flow, *Networks and Heterogeneous Media*, **1** (2006), 275–294.

[16] M. Herty and M. Rascle, Coupling conditions for a class of second-order models for traffic flow, *SIAM Journal on Mathematical Analysis*, **38** (2006), 595–616.

[17] W.-L. Jin, Q.-J. Gan and J.-P. Lebacque, A kinematic wave theory of capacity drop, *Transportation Research Part B: Methodological*, **81** (2015), 316–329.

[18] W. Jin and H. Zhang, On the distribution schemes for determining flows through a merge, *Transportation Research Part B: Methodological*, **37** (2003), 521–540.

[19] O. Kolb, *Simulation and Optimization of Gas and Water Supply Networks*, PhD thesis, TU Darmstadt, 2011.

[20] O. Kolb and J. Lang, Simulation and continuous optimization, in *"Mathematical Optimization of Water Networks"* (eds. A. Martin, K. Klamroth, J. Lang, G. Leugering, A. Morsi, M. Oberlack, M. Ostrowski and R. Rosen), Springer Basel, **162** (2012), 17–33.

[21] L. Leclercq, V. L. Knoop, F. Marczak and S. P. Hoogendoorn, Capacity drops at merges: New analytical investigations, *Transportation Research Part C: Emerging Technologies*, **62** (2016), 171–181.

[22] M. J. Lighthill and G. B. Whitham, On kinematic waves. II. A theory of traffic flow on long crowded roads, *Royal Society of London Proceedings Series A*, **229** (1955), 317–345.

[23] C. Parzani and C. Buisson, Second-order model and capacity drop at merge, *Transportation Research Record: Journal of the Transportation Research Board*, **2315** (2012), 25–34.

[24] B. Piccoli, K. Han, T. L. Friesz, T. Yao and J. Tang, Second-order models and traffic data from mobile sensors, *Transportation Research Part C: Emerging Technologies*, **52** (2015), 32–56.

[25] J. Reilly, S. Samaranayake, M. L. Delle Monache, W. Krichene, P. Goatin and A. M. Bayen, Adjoint-based optimization on a network of discretized scalar conservation laws with applications to coordinated ramp metering, *Journal of Optimization Theory and Applications*, **167** (2015), 733–760.

[26] F. Siebel, W. Mauser, S. Moutari and M. Rascle, Balanced vehicular traffic at a bottleneck, *Mathematical and Computer Modelling*, **49** (2009), 689–702.

[27] P. Spellucci, A new technique for inconsistent QP problems in the SQP method, *Mathematical Methods of Operations Research*, **47** (1998), 355–400.

[28] P. Spellucci, An SQP method for general nonlinear programs using only equality constrained subproblems, *Mathematical Programming*, **82** (1998), 413–448.

[29] A. Srivastava and N. Geroliminis, Empirical observations of capacity drop in freeway merges with ramp control and integration in a first-order model, *Transportation Research Part C: Emerging Technologies*, **30** (2013), 161–177.

[30] M. Treiber and A. Kesting, *Traffic Flow Dynamics*, Data, models and simulation, Translated by Treiber and Christian Thiemann, Springer, Heidelberg, 2013.

Received November 2016; revised February 2017.

E-mail address: kolb@uni-mannheim.de
E-mail address: goettlich@uni-mannheim.de
E-mail address: paola.goatin@inria.fr